The Astrophysical Journal, 693:1346–1359, 2009 March 10 doi:10.1088/0004-637X/693/2/1346

PRESSURE RELATIONS AND VERTICAL EQUILIBRIUM IN THE TURBULENT, MULTIPHASE INTERSTELLAR MEDIUM

Hiroshi Koyama[1] and Eve C. Ostriker
Department of Astronomy, University of Maryland, College Park, MD 20742, USA; hkoyama@astro.umd.edu, ostriker@astro.umd.edu
Received 2008 October 3; accepted 2008 December 10; published 2009 March 6

ABSTRACT

We use numerical simulations of turbulent, multiphase, self-gravitating gas orbiting in the disks of model galaxies to study the relationships among pressure, the vertical distribution of gas, and the relative proportions of dense and diffuse gas. A common assumption is that the interstellar medium (ISM) is in vertical hydrostatic equilibrium. We show that the disk height and mean midplane pressure in our multiphase, turbulent simulations are indeed consistent with effective hydrostatic equilibrium, provided that the turbulent contribution to the vertical velocity dispersion and the gas self-gravity are included. Although vertical hydrostatic equilibrium gives a good estimate for the mean midplane pressure $\langle P\rangle_{\rm midplane}$, this does not represent the pressure experienced by most of the ISM. Mass-weighted mean pressures $\langle P\rangle_{\rho}$ are typically an order of magnitude higher than $\langle P\rangle_{\rm midplane}$ because self-gravity concentrates gas and increases the pressure in individual clouds without raising the ambient pressure. We also investigate the ratio $R_{\rm mol} = M_{\rm H_2}/M_{\rm H\,I}$ for our hydrodynamic simulations. Blitz & Rosolowsky showed that $R_{\rm mol}$ is proportional to the estimated midplane pressure in a number of systems. We find that for model series in which the epicyclic frequency κ and gas surface density Σ vary together as $\kappa \propto \Sigma$, we recover the empirical relation. For other model series in which κ and Σ are varied independently, the midplane pressure (or Σ) and $R_{\rm mol}$ are not well correlated. We conclude that the molecular fraction—and hence the star formation rate—of a galactic disk inherently depends on its rotational state, not just the local values of Σ and the stellar density ρ_*. The empirical result $R_{\rm mol} \propto \langle P\rangle_{\rm midplane}$ implies that the three "environmental parameters" κ, Σ, and ρ_* are interdependent in real galaxies, presumably as a consequence of evolution: real galaxies tend toward states with Toomre Q parameter near unity. Finally, we note that $R_{\rm mol}$ in static comparison models far exceeds both the values in our turbulent hydrodynamic simulations and observed values of $R_{\rm mol}$, when $\Sigma > 10\,M_\odot$ pc^{-2}, indicating that incorporation of turbulence is crucial to obtaining a realistic molecular fraction in numerical models of the ISM.

Key words: galaxies: ISM – hydrodynamics – instabilities – ISM: general – methods: numerical – stars: formation – turbulence

Online-only material: color figure

1. INTRODUCTION

All phases of the interstellar medium (ISM) are turbulent, and this turbulence has many effects. In the astrophysical literature, turbulence is often treated as yielding a simple addition to the thermal pressure, $P_{\rm total} = \rho(c_s^2 + v_{\rm turb}^2)$, where $v_{\rm turb}^2$ is the dispersion in the (one-dimensional) turbulent velocity, and $c_s^2 = P/\rho = fk_{\rm B}T/\mu$ for gas with a total number density fn and mass density μn. This approach is often adopted when analyzing the stratification of interstellar gas clouds and the ISM as a whole, with the combined pressure gradients taken to balance the gravitational force per unit volume such that hydrostatic equilibrium is maintained by the total pressure. The turbulent pressure is believed to be especially important in the cold components of the ISM, for which observed linewidths far exceed the values of c_s inferred from excitation of atomic and molecular lines.

Models of effective hydrostatic equilibrium in the vertical direction, usually assuming that the turbulent and thermal velocity dispersions are constants independent of height, are often applied to observations of the large-scale Galactic ISM, and to observations of the ISM in external galaxies (e.g., Lockman & Gehman 1991; Malhotra 1994, 1995; Combes & Becquaert 1997; Olling & Merrifield 2000; Narayan & Jog 2002; Dalcanton et al. 2004; Blitz & Rosolowsky 2004, 2006; Kasparova & Zasov 2008). For example, Narayan & Jog (2002) showed that the observed atomic and molecular disk thicknesses in the Milky Way can be fit well by assuming effective hydrostatic equilibrium, and accounting for both the gas self-gravity and the external gravitational potential of stars and dark matter. Blitz & Rosolowsky (2004, 2006, hereafter BR06) used a simplified approach to hydrostatic equilibrium in order to estimate the midplane gas pressure in a sample of disk galaxies, adopting a single velocity dispersion for the gas, treating the gravitational potential as dominated by the stars, and assuming that the stellar disk's scale height is independent of radius. Kasparova & Zasov (2008) extended the analysis of BR06 but instead of adopting a constant scale height for the stellar disk, they assumed that the velocity dispersion for the stars is consistent with a state of marginal gravitational instability (with the Toomre parameter $Q_* = 1.5$) for the corresponding stellar surface density. They then assumed hydrostatic equilibrium for all (gaseous and stellar) components separately, and computed the self-consistent midplane pressure, finding differences of order 30%–40% from the simplified BR06 approach. Although widely adopted, the effective hydrostatic equilibrium model for the large-scale ISM has not, to our knowledge, been explicitly verified using actual turbulent flows. One of the goals of this work is to test this formulation systematically, using the solutions of time-dependent numerical hydrodynamic simulations of turbulent, multiphase gas.

[1] Current address: High-Performance Computing Team, Integrated Simulation of Living Matter Group, Riken, 61-1 Ono-cho, Tsurumi, Yokohama 230-0046, Japan; hkoyama@riken.jp.

In addition to providing support against gravity, pressure also affects the phase balance in the ISM. For a static system at a given mean density $\bar{n}$, changing the pressure alters the proportions of mass divided between dense clouds and diffuse intercloud medium; e.g., for cold and warm components in pressure equilibrium, the mass ratio of cold to warm gas is $M_{\rm cold}/M_{\rm warm} = [\bar{n}/n_{\rm warm} - 1]/[1 - \bar{n}/n_{\rm cold}] = [\bar{n}kT_{\rm warm} - P]/[P - \bar{n}kT_{\rm cold}]$. The mean density itself, however, depends on pressure through the condition of vertical hydrostatic equilibrium. Turbulent pressure, as it affects the response to external and self-gravity, can be expected to change both the mean density and the mass fractions of dense and diffuse gas. Here, we investigate these effects quantitatively.

The fraction of ISM mass in dense gas is important from the point of view of galactic evolution, since this component is the immediate precursor to star formation. A recent observational study of external disk galaxies by BR06 identified a linear relationship between the mean ratio of molecular-to-atomic mass, $R_{\rm mol}$, and an estimate for the total midplane pressure proportional to $\sqrt{\rho_* \Sigma}$, where ρ_* is the stellar volume density and Σ is the total gaseous surface density. BR06 propose that the molecular fractions in widely varying types of galaxies—and hence their respective star formation efficiencies—are therefore determined essentially by a single parameter: the midplane pressure. To investigate this proposal, we use multiphase turbulence simulations in which we independently vary the input galactic "environmental" parameters. The observational study of BR06 focused on the dependence of $R_{\rm mol}$ on ρ_* and Σ, but another important—and independent—environmental parameter is the angular rotation rate Ω (and the associated epicyclic frequency $\kappa^2 = R^{-3} d(\Omega^2 R^4)/dR$). Using our data sets from turbulent simulations, we compare the pressure estimate of BR06 to the true value of the pressure, and also test how $R_{\rm mol}$ relates to the mean pressure measured in two different ways.

We note that a number of recent numerical studies have investigated the formation of ISM structures with internal densities reaching those similar to giant molecular clouds (GMCs). Some studies (e.g., Koyama & Inutsuka 2002; Heitsch et al. 2005, 2006; Hennebelle & Audit 2007; Hennebelle et al. 2007, 2008; Vázquez-Semadeni et al. 2007) have focused on how this may occur as a consequence of the collision of large-scale high-velocity flows that shock and cool, becoming turbulent at the same time. Other studies have focused on the ability of self-gravitating instabilities to induce converging flows over sufficiently large scales that massive, high-column density structures similar to observed GMCs are created (e.g., Kim & Ostriker 2001, 2007; Li et al. 2005, 2006); these models include the galactic shear and rotation that are important on these large scales, and in some cases also include magnetic effects (e.g., Kim et al. 2002, 2003). As spiral arms are observed to be strongly associated with high molecular fractions and star formation, some studies have focused on the interaction between large-scale spiral shocks and self-gravity in inducing GMC formation (e.g., Kim & Ostriker 2002, 2006; Dobbs 2008). The details of conversion from diffuse to dense gas by cooling downstream from spiral shock fronts have also recently been studied in the absence of self-gravity (e.g., Dobbs et al. 2008; Kim et al. 2008). Taken together, these and other recent studies have shown that significant quantities of dense gas form naturally as a result of large-scale ISM dynamical processes. Of course, dense gas in the ISM is also returned to the diffuse phases by the energetic inputs from star formation. In the present work, by incorporating feedback, we are able to evolve our models until a quasi-steady state is reached. This enables an analysis of the correlations among statistical properties of the system, in terms of their influence on the fraction of dense gas when the system has reach a quasi-steady state of cloud formation and destruction.

This paper is organized as follows: in Section 2 we briefly summarize our numerical methods. The specification of model parameters and the results of statistical analysis in comparison to the vertical-equilibrium approximation are presented in Section 3. In Section 4, we discuss the molecular fraction and investigate how it relates to the ISM pressure in our models. We summarize our results and discuss implications for ISM structure and evolution in Section 5.

2. NUMERICAL METHODS

The analysis in this paper is based on time-dependent numerical hydrodynamic simulations of turbulent, multiphase, interstellar gas. Details of our numerical methods are presented in a companion paper (Koyama & Ostriker 2009, hereafter Paper I); here, we briefly summarize the model properties and parameterizations. The models we use are two dimensional, representing slices through the ISM in radial–vertical (R–z) planes. We include sheared galactic rotation, a radial gravitational force (the centrifugal force and gravity balance in the unperturbed state, which assumes a rotation curve $V_c = $ const.), and Coriolis forces in the equations of motion, as well as gaseous self-gravity and vertical gravity representing the potential of the stellar disk. The gas is treated as a single fluid in chemical equilibrium, and we include (volumetric) radiative heating and cooling processes as a function of density and temperature appropriate to the range $10 < T < 10^4$ K. The thermal processes we incorporate include photoelectric heating from small grains and polycyclic aromatic hydrocarbons, heating and ionization by cosmic rays and X-rays, heating by H_2 formation and destruction, atomic line cooling from Hydrogen Lyα, C II, O I, Fe II, and Si II, rovibrational line cooling from H_2 and CO, and atomic and molecular collisions with grains. We adopt shearing-periodic boundary conditions in the radial direction.

To drive turbulence, we also include a model of stellar feedback: within "H II regions" (which are defined by contours of the perturbed gravitational potential surrounding regions where the density has exceeded a specified threshold), the gas heating rate is increased by a factor of 1000. As a consequence, gas within these "H II regions" heats to temperatures $\sim 10^4$ K, irrespective of density. The detailed recipe for the feedback phenomenon is described in Paper I. Our aim is not to represent star formation feedback in a fully realistic manner, but to drive turbulence in a way similar to that which occurs within the dense ISM. In this sense, our feedback prescription is similar in spirit to simulations of GMCs in which turbulence is applied via arbitrary forcing functions (e.g., Stone et al. 1998; Mac Low 1999; Klessen et al. 2000). Thus, our results should be taken as demonstrating the physical importance of turbulence to setting properties such as the vertical thickness of the disk, not as giving quantitative predictions for what the value of the disk thickness, etc., should be.

3. MODEL SERIES AND RESULTS

In our local disk models, three free parameters are needed to characterize the "galactic environment": the total surface density of the gas Σ, the local epicyclic frequency κ, and the local stellar density ρ_*. As we assume a flat rotation curve, $\kappa = \sqrt{2}\Omega$ where

Ω is the angular rotation rate at the center of our domain. The stellar density is used in order to specify the vertical gravity $\mathbf{g}_* = -4\pi G\rho_* z\hat{z}$.

Following Paper I, we study four series of models to explore the parameter dependence of our results. For each series, we hold two quantities fixed and vary a third quantity, as follows.

1. Series Q: κ/Σ and $\sqrt{\rho_*}/\Sigma$ are constant while Σ varies;
2. Series K: κ and $\sqrt{\rho_*}/\Sigma$ are constant while Σ varies;
3. Series R: κ/Σ and ρ_* are constant while Σ varies;
4. Series S: Σ and ρ_* are constant while κ (and Ω) varies.

Since Toomre's parameter is proportional to κ/Σ, Series Q and R would have constant gaseous $Q = \kappa c_s/(\pi G\Sigma)$ if the sound speed c_s were constant. The Q and R Series correspond to values of $Q = 2.1(c_s/7\mathrm{kms}^{-1})$. Assuming a constant stellar velocity dispersion, $\Sigma_* \propto \sqrt{\rho_*}$, so that the stellar Toomre parameter (hereafter Q_*) would also have the same value for all members of Series Q. In all members of the R and S Series and in the $\Sigma = 15.0\,M_\odot\,\mathrm{pc}^{-2}$ models of the Q and K Series, we take $\rho_* = 0.14\,M_\odot\,\mathrm{pc}^{-3}$. In the K Series, we use $\kappa = 62.4\,\mathrm{kms}^{-1}\mathrm{kpc}^{-1}$, while in the S Series we use $\Sigma = 15.0\,M_\odot\,\mathrm{pc}^{-2}$.

This paper focuses on how turbulence affects the vertical structure of the galactic ISM. An important aspect of our studies is to understand how the results differ from the situation in which turbulence is absent. Thus, as baselines for comparison, we have two vertical nonturbulent model series: one in which the gas and stellar surface densities are proportional (Series HSP), and one in which the stellar surface density is constant (Series HSC). These correspond to dynamical Series Q and K (for HSP) and Series R (for HSC), respectively. These models are one dimensional in the vertical (z) direction; each model represents the asymptotic hydrostatic equilibrium state which develops in the absence of any stellar feedback.

Figure 1 shows a snapshot of the gas pressure in a dynamical model from Series Q, compared to the hydrostatic model from Series HSP. The density and temperature are shown for the same snapshot in Figure 1 of Paper I. In the dynamical model, the pressure overall increases toward the midplane, but there are significant variations associated with structure in the gas; for the particular snapshot shown, there is also a high-pressure region near the left of the figure, which is associated with a locally heated star formation feedback region. The hydrostatic model shows a secular increase in pressure toward the midplane.

3.1. Vertical Scale Height

We begin by examining the vertical velocity dispersion of gas in all of the model series. Figure 2 shows space and time averages (weighted by mass) of both the thermal velocity dispersion $c_s = (P/\rho)^{1/2}$ (circles) and the combined thermal + turbulent velocity dispersion $\sigma_z = \sqrt{c_s^2 + v_z^2}$ (triangles). The four panels correspond to the Series Q, K, R, and S. In Series Q and R, the mean thermal velocity dispersion decreases with increasing surface density. The reason for this is that the mass fraction of cold, dense gas increases with Σ in all of these models (see Paper I). This is because gravity is lower, and gas is less compressed (both vertically, and horizontally by self-gravity), at low Σ. In Series K, on the other hand, the mean thermal speed has a local minimum at intermediate Σ. Again, this can be understood in terms of the mass fraction of warm gas, which is largest at low and high Σ (see Paper I) in this series; at high Σ, the model is extremely active in terms of feedback because (with constant κ) the disk is quite unstable gravitationally. For all the series in which Σ is the variable parameter (i.e., Q, K, and R), the turbulent part of the total velocity dispersion increases with Σ; this is because the higher-Σ models have higher feedback rates, and therefore increasing (or flat) turbulence levels. For Series S (with constant Σ), the turbulence decreases as Ω increases, as high κ stabilizes the disk and prevents gravitational collapse and feedback (see Figure 11 in Paper I). For all series, the (mass-weighted) turbulent vertical velocity dispersion approaches or exceeds the (mass-weighted) thermal velocity dispersion for some part of parameter space, so that turbulent support of gas in the vertical gravitational field is expected to be important.

Next, we measure (for all series) the vertical scale height, using the following averaging:

$$H_{\mathrm{ave}} = \sqrt{\frac{\sum_{\mathrm{allzones}} \rho z^2}{\sum_{\mathrm{allzones}} \rho}} \tag{1}$$

where z is the vertical coordinate relative to the midplane. We further average the values of H_{ave} over time. In order to test whether the velocity dispersion can be used to obtain an accurate measure of the scale height, we also compute "estimated" vertical scale heights defined as

$$H_{\mathrm{est}} = \frac{1}{\sqrt{2\pi}} \frac{\sigma_z^2}{G\Sigma + \left[(G\Sigma)^2 + 2G\rho_*\sigma_z^2\right]^{1/2}} = \frac{\sigma_z}{\sqrt{4\pi G\rho_*}} \frac{1}{A + [A^2+1]^{1/2}} \tag{2}$$

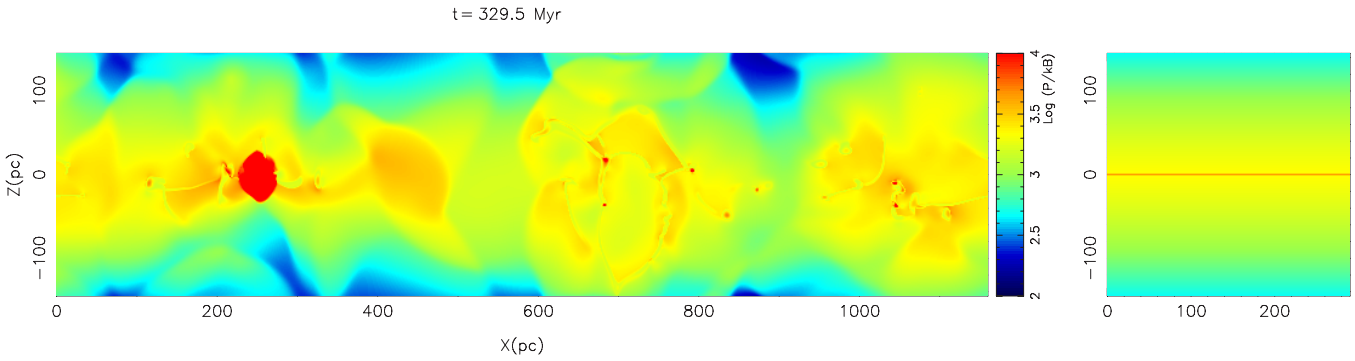

Figure 1. Left: snapshot of gas pressure (logarithmic color scale) from Model Q11 simulation. For comparison, the right panel shows the pressure in the hydrostatic model (HSP11) that has the same total gas surface density Σ and stellar density ρ_* as Model Q11.

(A color version of this figure is available in the online journal.)

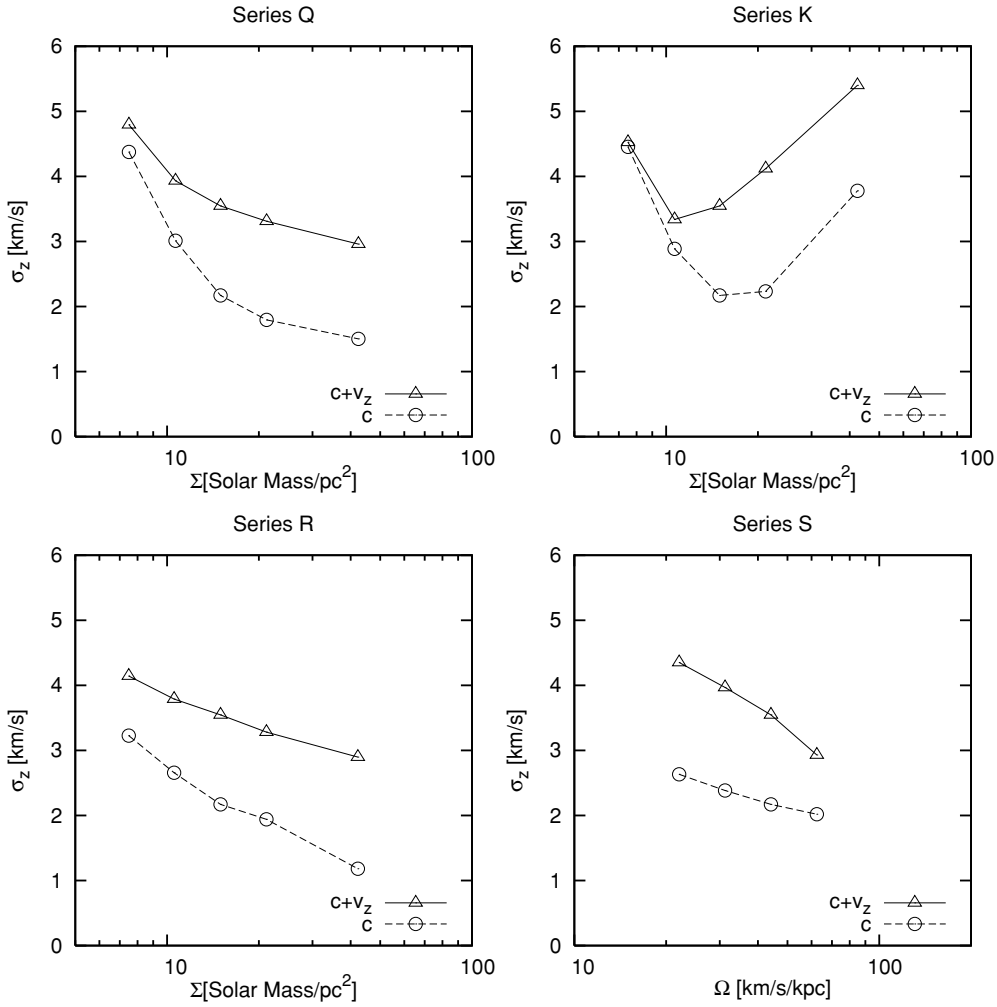

Figure 2. Mean vertical velocity dispersion, weighted by mass. Both the thermal c_s (circles) and the total (thermal + turbulent) $\sigma_z = \sqrt{c_s^2 + v_z^2}$ (triangles) dispersions are shown for all series.

$$H_{\rm est} = \begin{cases} \dfrac{\sigma_z}{\sqrt{4\pi G\rho_*}} & (\Sigma \to 0) \\ \dfrac{\sigma_z^2}{\sqrt{8\pi} G\Sigma} & (\rho_* \to 0). \end{cases} \quad (3)$$

This formula (see the appendix for derivation) accounts for both gas self-gravity and stellar gravity; the limiting forms are for negligible gaseous and stellar gravity, respectively.

In Equation (2), A is a dimensionless factor that measures the relative densities of the gaseous and stellar disks,

$$A \equiv \sqrt{\frac{G\Sigma^2}{2\rho_*\sigma_z^2}} = \frac{\Sigma\, c_{*,z}}{\Sigma_*\, \sigma_z \sqrt{\pi}}. \quad (4)$$

The latter expression treats the stellar disk as an isothermal self-gravitating equilibrium, with $H_* = c_{*,z}^2/(\pi G\Sigma_*)$, and shows that $A \sim Q_*/Q$ (assuming that vertical and radial velocity dispersions are proportional). Equation (2) may be thought of as an extension of the usual non-self-gravitating scale height formula to account for the gravity of the gas. Since $A > 0$, the correction factor depending on A is always less than 1. If the gas disk is much more gravitationally unstable than the stellar disk ($A \sim Q_*/Q \gg 1$), the correction factor is large; otherwise, the correction factor is of order unity.

Figure 3 shows the measured ($H_{\rm ave}$) and "predicted" ($H_{\rm est}$) disk scale heights for all series of hydrodynamic models. For $H_{\rm est}$, we show results using for σ_z either the thermal velocity dispersion ($\sigma_z = c_s$; subscript c) or the total velocity dispersion ($\sigma_z^2 = c_s^2 + v_z^2$; subscript $c + v_z$). To show how turbulence contributes to setting the disk thickness, $H_{\rm ave}$ is also shown for the hydrostatic models. The difference between $H_{\rm ave}$ in hydrostatic and hydrodynamic models can be quite large, up to a factor of 10 in some cases. We note that $H_{\rm ave}$ of the hydrostatic models (filled boxes) differs from $H_{{\rm est},c}$ (open circles) because the mass-weighted mean sound speed differs for hydrostatic and hydrodynamic models.

Overall, Figure 3 shows that the estimate for scale height $H_{{\rm est},c+v_z}$ that includes turbulence traces the measured $H_{\rm ave}$ quite well, for all the series. The difference between $H_{{\rm est},c}$ and $H_{{\rm est},c+v_z}$ increases with increasing Σ, with quite large differences for some of the models in Series Q and R. This indicates that high surface density disks are supported largely by turbulent velocities, in these cases. To facilitate comparisons between estimated and measured value of the scale height, in the lower part of each panel we also show the ratios $H_{{\rm est},c}/H_{\rm ave}$ (circles) and $H_{{\rm est},c+v_z}/H_{\rm ave}$ (triangles). At low values of Σ in Series Q, K, and R, both estimates of H exceed the true measured value. It is notable that where the turbulent contributions are large,

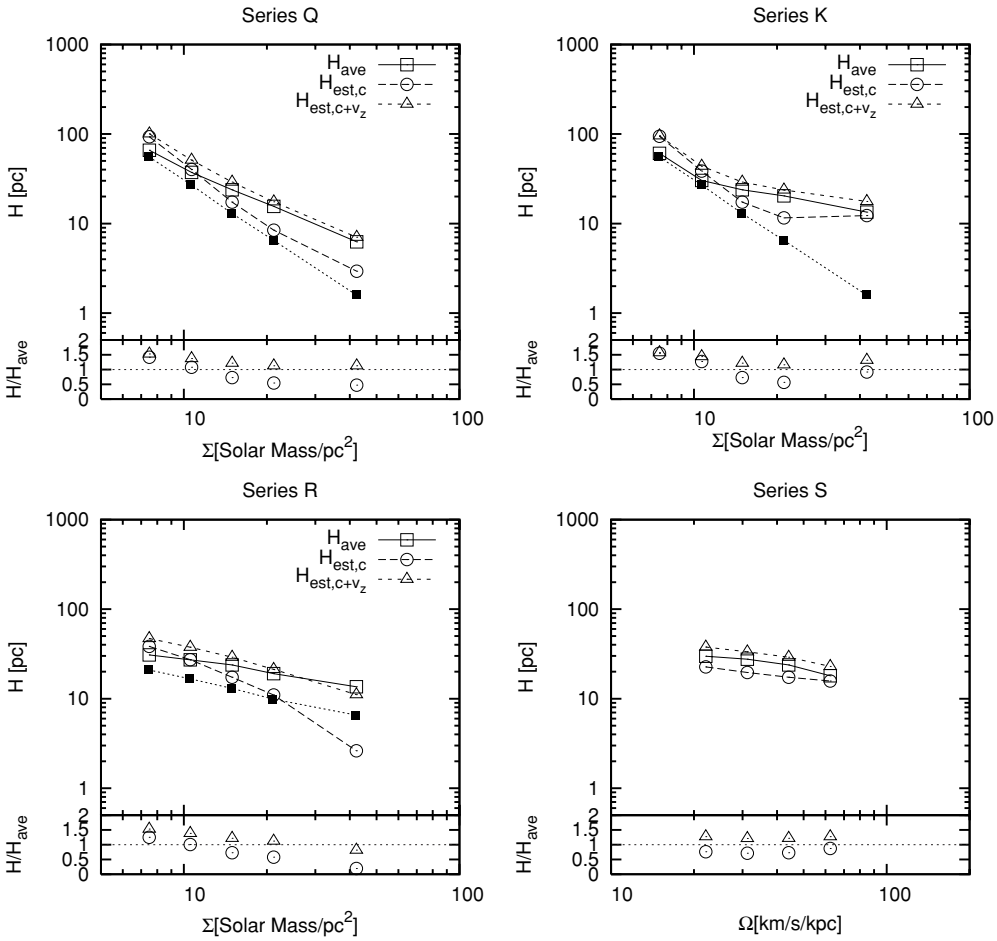

Figure 3. Disk scale heights, for all hydrodynamic and hydrostatic models. Open boxes denote the directly measured scale height (see Equation 1) for all hydrodynamic series. Filled boxes show the measured scale height for corresponding hydrostatic models (HSP for Series K and Q, HSC for Series R). Open circles and triangles show the estimated scale heights (see Equation 2) using thermal and thermal plus turbulent velocity for σ_z, respectively. The bottom part of each panel shows the ratio of estimated scale heights to direct measurements.

at high Σ in Series Q, K, and R, the estimated and measured disk thicknesses are in quite good agreement (within $\sim$ 10%–20%). Thus, we conclude that if measurements of the vertical velocity dispersion together with the gaseous surface density and stellar surface density can be made observationally, they can be combined to yield an accurate estimate of the gas disk's thickness.

3.2. Gas Pressure

The gaseous pressure, like the scale height, is often difficult to measure directly. As a consequence, other proxies are often used to obtain an estimate of the value of the pressure, with an assumption that vertical equilibrium is satisfied. Here, we test how well such pressure estimates agree with the directly measured pressure, for our multiphase turbulent models.

Figure 4 shows for all models in all hydrodynamic series the average gas pressure. We consider two different ways of averaging: weighting by mass $\langle P \rangle_\rho$ (open box), and weighting by volume $\langle P \rangle_{\rm midplane}$ (open circle). The value $\langle P \rangle_\rho$ is interesting because it characterizes the value of pressure experienced by the average atom or molecule, whereas $\langle P \rangle_{\rm midplane}$ is interesting because it represents the pressure in the diffuse (non-self-gravitating) part of the ISM that is closest to star forming regions.

The mass- and volume-weighted averages are defined by the following:

$$\langle P \rangle_\rho = \frac{\int P dm}{\int dm}, \tag{5}$$

$$\langle P \rangle_{\rm midplane} = \int \frac{P_{\frac{N_z}{2}} + P_{\frac{N_z}{2}+1}}{2} \frac{dx}{L_x}. \tag{6}$$

For $\langle P \rangle_\rho$, all zones in the domain are included, while for $\langle P \rangle_{\rm midplane}$, the subscripts $\frac{N_z}{2}$ and $\frac{N_z}{2}+1$ indicate that only zones in the two horizontal planes closest to the midplane are included. Time averaging is applied in all models after the above space averaging. We also show the same pressure averages for the hydrostatic series (filled box and filled circle). Interestingly, in the hydrodynamic models $\langle P \rangle_\rho$ always exceeds $\langle P \rangle_{\rm midplane}$ by a large factor of $\sim$ 10. This indicates that self-gravity is important in increasing the pressure above the "ambient" value, for much of the gas. Pressures cannot exceed the ambient midplane value without horizontal gradients, which are balanced by the gravity within individual clouds (see Figure 1). In the hydrostatic models, $\langle P \rangle_\rho$ (filled boxes) is generally slightly below $\langle P \rangle_{\rm midplane}$ (filled circles), because the pressure at the midplane is the maximum within any system, and weighting by mass includes lower-pressure gas which reduces the average.

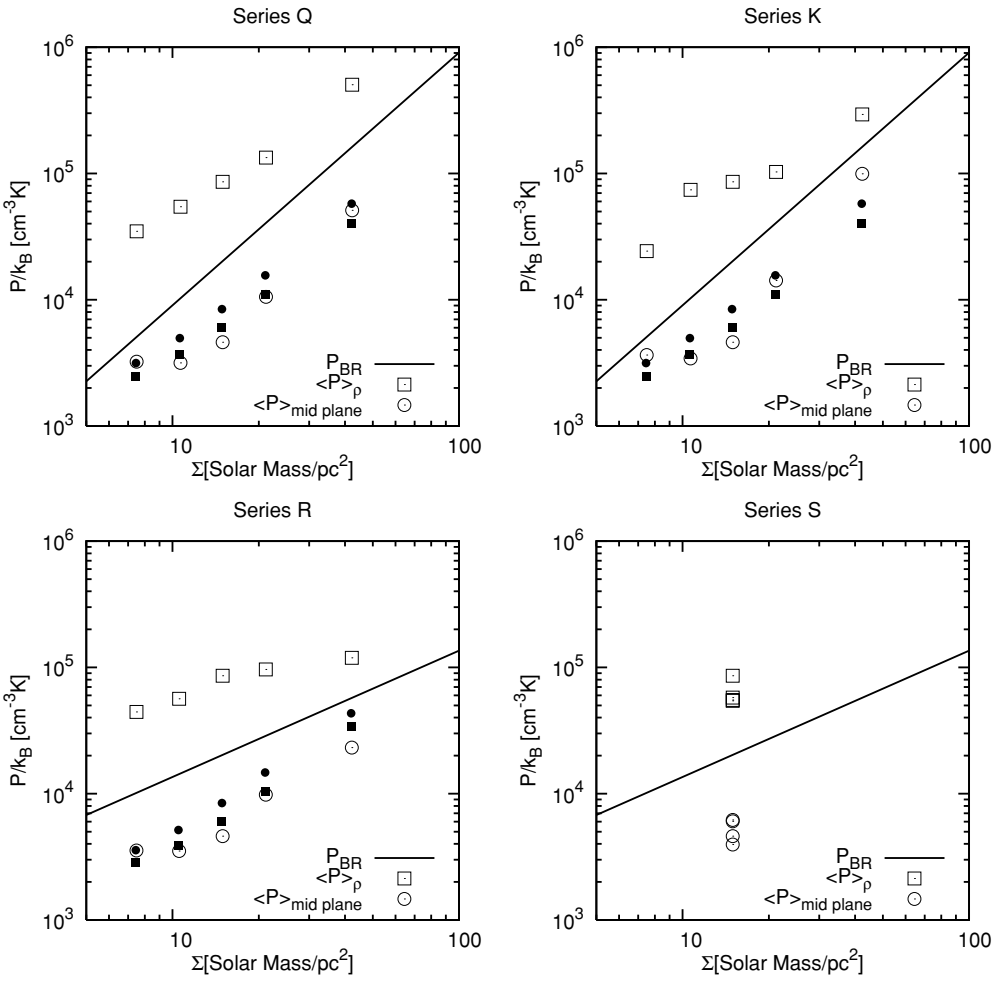

Figure 4. Gas pressure averages for all series. Open boxes show mass-weighted averages and open circles show the midplane pressure, for hydrodynamic models. Filled boxes and filled circles show the same for hydrostatic models. The pressure estimate of BR06 is also indicated as a solid line.

(Note that for the hydrostatic models, there are no horizontal gradients in any quantities; see Figure 1.) Except in the most active disks, the mass-weighted averages for the hydrostatic models are close to the midplane values for the hydrodynamic models. In Figure 4 we also display the pressure estimate of BR06 (solid line) defined as

$$P_{\rm BR} = \Sigma v \sqrt{2G\rho_*}, \tag{7}$$

where $v = 8$ km s^{-1} is adopted. This line falls between $\langle P \rangle_\rho$ and $\langle P \rangle_{\rm midplane}$ for all the hydrodynamic series.

For hydrostatic Series HSP (shown in the Series Q and K panels), the slope of the midplane pressure is close to that predicted by Equation (7), while being offset to lower P by a factor of 2–3. The difference in slope is because the medium has multiple phases, rather than a single phase at a given thermal sound speed. The offset is because (1) much of the mass in the hydrostatic models is at low temperatures, for which the sound speed is well below 8 km s^{-1} and (2) Equation (7) does not include the gaseous vertical gravity, which is comparable to the stellar gravity when vertical velocity dispersion is low and the disk is very thin (see below). These effects push P in opposite directions, and hence partially compensate each other. For hydrostatic series HSC (shown in the Series R panel), the prediction of Equation (7) departs significantly from the slope of the midplane pressure results, because in the HSC series (which has ρ_* constant) vertical gravity is strongly dominated by gas rather than the stellar component at large Σ.

In Section 3.1, we defined an "average" vertical equilibrium using the total surface density and the total vertical velocity dispersion, and showed that this could yield an accurate measurement of the disk thickness. The same model (see the Appendix) can be used to estimate a midplane "effective hydrostatic pressure," which we can compare to measured values. If H is the scale height, then in equilibrium the mean midplane gas density is $\rho_0 = \Sigma/(\sqrt{2\pi}H)$. Using the total velocity dispersion, the predicted total gas pressure at the midplane is then given by $P_{0,\rm tot} = \sigma_z^2 \rho_0$, which using Equation (2) gives

$$\begin{aligned} P_{0,\rm tot} &= \frac{\sigma_z^2 \Sigma}{\sqrt{2\pi}\, H_{{\rm est},c+v_z}} = \Sigma\left(G\Sigma + \left[(G\Sigma)^2 + 2G\rho_* \sigma_z^2\right]^{1/2}\right) \\ &= \Sigma\sigma_z\sqrt{2G\rho_*}(A + \sqrt{A^2+1}). \end{aligned} \tag{8}$$

Equation (8) corresponds to an extension of the pressure estimate formula of BR06 using the inverse of the A-dependent correction factor that appears in the scale height estimate (Equation 2). This correction factor is greater than 1.

Equation (8) gives an estimate of the total midplane pressure, but the thermal pressure should represent only a fraction $\langle c_s^2 \rangle / \langle c_s^2 + v_z^2 \rangle = 1 - \langle v_z^2 \rangle / \sigma_z^2$ of $P_{0,\rm tot}$, where $\langle v_z^2 \rangle^{1/2}$ is the mass-weighted rms turbulent velocity dispersion in the vertical

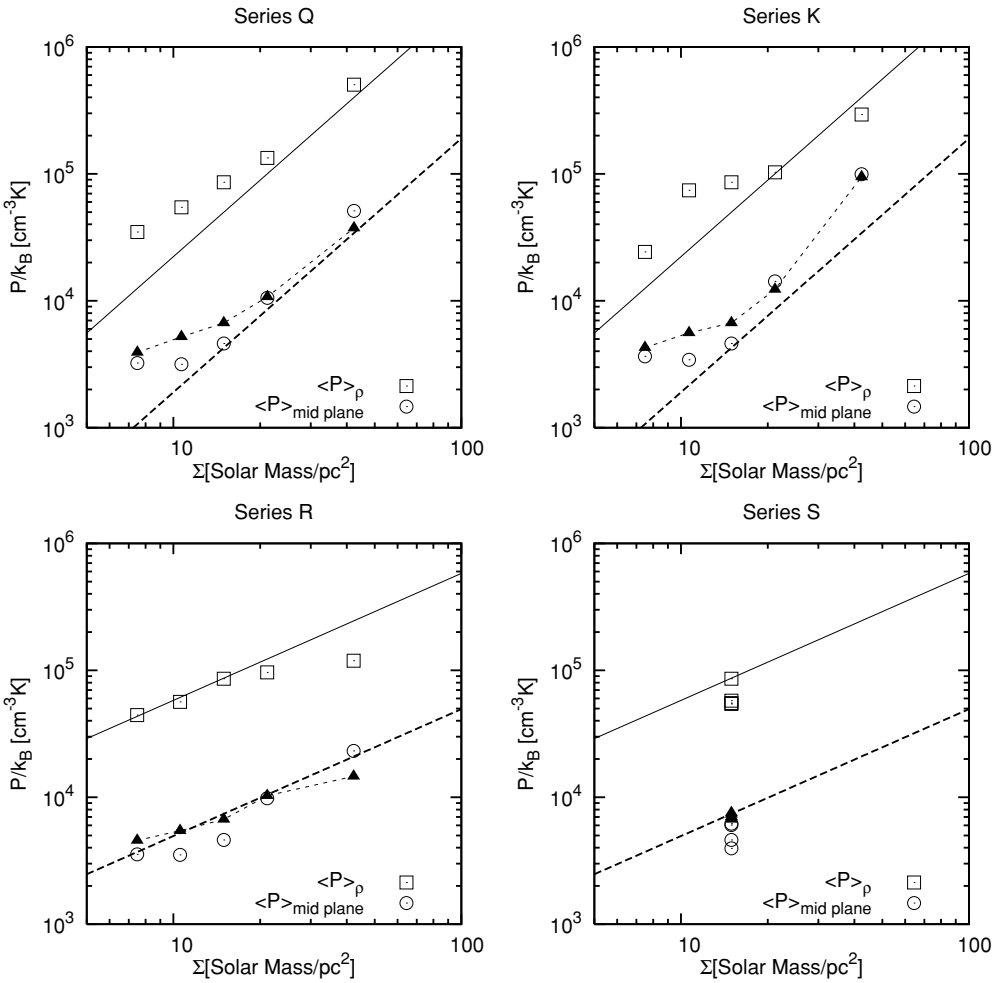

Figure 5. Measured, fitted, and estimated gas pressures. Open boxes and circles are the same as in Figure 4. Solid and dashed lines are the corresponding fits to Equation (10). Our vertical-equilibrium midplane thermal pressure estimate (Equation 9) is plotted as filled triangles.

direction. Thus, our estimate of the mean thermal pressure at the midplane is

$$P_{0,\rm th} = \langle c_s^2 \rangle \frac{\Sigma}{\sqrt{2\pi}\, H_{{\rm est},c+v_z}} = \Sigma \frac{\langle c_s^2 \rangle}{\sigma_z} \sqrt{2G\rho_*}(A + \sqrt{A^2+1}). \quad (9)$$

In Figure 5, we compare the pressure estimate from Equation (9, filled triangles) with the measurements of midplane pressure. At large Σ, the agreement is quite good, while at low Σ the estimated midplane pressures lie slightly above the measured values. This behavior is similar to our results for estimated scale heights, which were in best agreement with the measured $H_{\rm ave}$ at large Σ (where the dense gas dominates the mass, and the velocity dispersion is turbulence dominated).

For all the series in which Σ is the independent variable, we have fit the measured gas pressure to the formula

$$P/k_{\rm B} = D\sqrt{\frac{\rho_*}{M_\odot\,{\rm pc}^{-3}}}\left(\frac{\Sigma}{M_\odot\,{\rm pc}^{-2}}\right). \quad (10)$$

For $\langle P \rangle_\rho$ and $\langle P \rangle_{\rm midplane}$, we find the respective coefficients are $D_\rho = 1.3 \times 10^4\,{\rm K\,cm^{-3}}$ and $D_{\rm midplane} = 1.1 \times 10^3\,{\rm K\,cm^{-3}}$. The largest and smallest surface density models are excluded in the fits. The results of the fits are displayed as solid and dashed lines, respectively, in Figure 5. To compare with the BR06 formula, we also fit $\langle P \rangle_\rho$ and $\langle P \rangle_{\rm midplane}$ to $P = C\Sigma v\sqrt{2G\rho_*}$ with $v = 8\ {\rm km\ s^{-1}}$. We find $C_\rho = 3.6$ and $C_{\rm midplane} = 0.3$; i.e., the BR06 formula for pressure yields values that are typically a factor of ~ 3 larger than our measured midplane pressures, and a factor of ~ 4 below the mass-weighted mean values of pressure. As noted above, the mass-weighted average pressures are about 10 times larger than the midplane pressures; this is evident in the ratio of the fitting coefficients.

Finally, we note that for most models (except at low Σ), the measured midplane pressure exceeds the maximum pressure of the warm neutral medium, $P_{w,\rm max}/k_{\rm B} = 5.5 \times 10^3\,{\rm K\,cm^{-3}}$ for our adopted heating and cooling functions. Dense clouds that are externally confined by the warm medium cannot have pressure exceeding $P_{w,\rm max}$ unless they are internally stratified (implying they are self-gravitating); thus, $P_{w,\rm max}$ is the largest the midplane pressure could be in the absence of self-gravity. Equation (9) can be solved for Σ in terms of the midplane value of $P_{0,\rm th}$. The maximum surface density for an atomic-only disk without self-gravitating clouds is then obtained by setting $P_{0,\rm th} \to P_{w,\rm max}$, with the result $\Sigma \to (P_{w,\rm max}/G)^{1/2}\sigma_z/c_s$ times a function of A that varies between 0.3 and 0.6 for $A = 0.1$–1. Assuming $\sigma_z/c_s \sim \sqrt{2}$ and taking $P_{w,\rm max}/k_{\rm B} = 5.5 \times 10^3\,{\rm K\,cm^{-3}}$, the maximum surface density for a pure-atomic disk is $\sim 10\,M_\odot\,{\rm pc}^{-2}$; this is consistent with the saturation levels for H I gas observed, e.g., by Wong & Blitz (2002). Since the measured midplane pressure is a volume-weighted sum of the pressures in different phases, a mean value exceeding $P_{w,\rm max}$ implies that

Table 1
Processes and Parameters for H_2 Formation/Dissociation

Parameter	Value	
Formation of H_2 on dust grains	$R_f = 6 \times 10^{-17}(T/300)^{0.5} S(T) \mathrm{cm^3 s^{-1}}$	[1]
Sticking probability	$S(T) = [1 + 0.04(T + T_d)^{0.5} + 2 \times 10^{-3} T + 8 \times 10^{-6} T^2]^{-1}$	[1]
Photodissociation rate	$R_{\rm pump} = 3.4 \times 10^{-10} G_0 \beta(\tau) \exp(-2.5 A_v) \mathrm{s^{-1}}$	[1]
Self-shielding function	$\beta(\tau) \cdots$	[1]
Optical depth	$\tau = 1.2 \times 10^{-14} f N_{\rm H} \delta v_d^{-1}$	[1]
Cosmic-ray dissociation	$\zeta_{\rm CR}^{\rm H_2} = 2.29 \zeta_{\rm CR}^{\rm H}$	[2]
Turbulent line broadening	$\delta v_d = 1 \,\mathrm{km\,s^{-1}} \left(\frac{N_{\rm H}/n}{1\,\mathrm{pc}}\right)^{0.5}$	[3]
Visual attenuation	$A_v \equiv N_{\rm H}/1.5 \times 10^{21} \mathrm{cm^{-2}}$	

References. [1] Tielens & Hollenbach (1985); [2] Hollenbach & McKee (1989); [3] Solomon et al. (1987).

self-gravitating dense clouds occupy a nonnegligible fraction of the midplane volume, $f_V = (M_{\rm dense}/M_{\rm diffuse})(\rho_{\rm diffuse}/\rho_{\rm dense})$, with $\langle P \rangle_{\rm midplane} = (P_{\rm dense} - P_{\rm diffuse}) f_V + P_{\rm diffuse}$. In the following section, we turn to a discussion of the relationship between the dense-to-diffuse mass ratio and global parameters.

4. AN APPLICATION: MOLECULAR MASS/PRESSURE RELATIONS

In this section, we explore relationships between the dense gas fraction and "environmental" conditions, including the gas pressure and the gas surface density. We are motivated by observations that show high molecular fractions in environments—including spiral arms and galactic center regions—where both the total gas surface density and stellar density are high. In particular, BR06 found for a number of disk systems that the mean ratio of molecular-to-atomic mass scales nearly linearly with the pressure estimate $P_{\rm BR}$ defined in Equation (7). Although our turbulent, multiphase simulations show that $P_{\rm BR}$ in fact overestimates the pressure of the typical volume element and underestimates the pressure of the typical mass element, $P_{\rm BR}$ nevertheless systematically increases in a similar way to both $\langle P \rangle_{\rm midplane}$ and $\langle P \rangle_\rho$. Thus, it is interesting to test how the dense-to-diffuse gas mass ratio depends on the true values of pressure. In addition to empirical results suggesting a relation between mass ratio and pressure, there are theoretical reasons that the mass ratio should depend on the mean gaseous surface density. For example, if atomic gas is converted to molecular clouds through gravitational instabilities on a timescale $t_{\rm form} \sim \sigma_{\rm H\,I}/(G\Sigma)$, and molecular clouds are destroyed by star formation on a timescale $t_{\rm dest}$, equating cloud formation and destruction rates implies $M_{\rm H_2}/M_{\rm H\,I} = t_{\rm dest}/t_{\rm form}$, which is proportional to Σ if the H I velocity dispersion and cloud destruction time are relatively constant. Thus, it is interesting to explore the dependence of $M_{\rm H_2}/M_{\rm H\,I}$ on the surface density—which appears in both the effective hydrostatic pressure and the rate of self-gravitating instabilities.

4.1. Molecular Gas

Although our numerical model does not directly include formation/dissociation processes of H_2, we can nevertheless relate our results to observed gas phases in an approximate way, using density as a proxy. Namely, we expect gravitationally bound dense clouds at $n > 100$ cm^{-3} to consist primarily of H_2, whereas diffuse gas at lower densities consists primarily of H I. We argue for this approximate identification based on the formation/dissociation equilibrium condition for H_2 molecules, which includes photodissociation and cosmic ray dissociation,

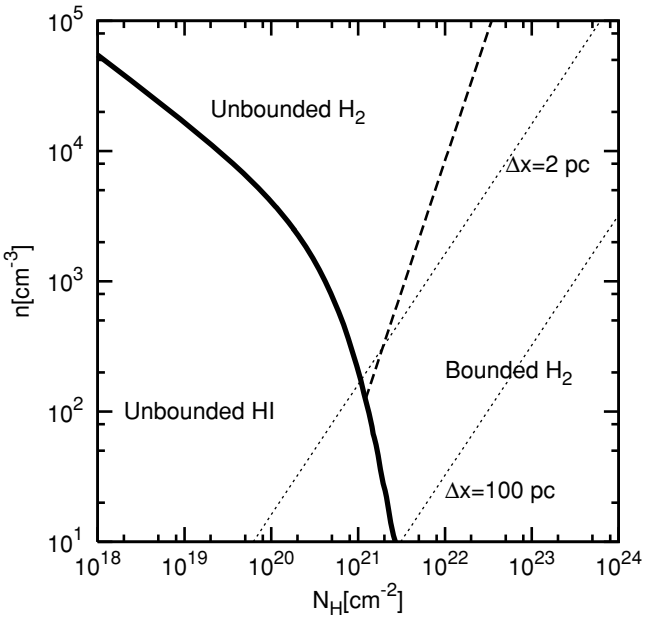

Figure 6. Phases in the density–column density plane. The solid line divides the area into predominantly H I at low $n_{\rm H}$ and $N_{\rm H}$, and predominantly H_2 at high $n_{\rm H}$ and $N_{\rm H}$, adopting molecule formation and destruction processes as described in the text. Shown as a dashed line is $N = nL_{\rm J}$, where $L_{\rm J}$ is the Jeans length at n for $T = 10$ K gas. The left- and right-hand sides of this line are gravitationally unbound and bound, respectively. Dotted lines show the typical resolution limit of the simulations $\Delta x = 2$ pc, and a maximum cloud scale of 100 pc.

and formation on dust grains:

$$\left(R_{\rm pump} + \zeta_{\rm CR}^{\rm H_2}\right) n f_{\rm mol} = R_f n^2 (1 - f_{\rm mol}) \qquad (11)$$

(Tielens & Hollenbach 1985). Here, $f_{\rm mol} \equiv 2n(\mathrm{H_2})/n$ is the molecular fraction, and $1 - f_{\rm mol} = n(\mathrm{H\,I})/n$ is the atomic fraction. The FUV dissociation rate is limited by shielding, which depends on the optical depth in H_2 lines and the extinction. Formation on grains depends on the sticking probability. The details of the terms involved are listed in Table 1. We adopt FUV field strength $G_0 = 1.7$, gas and dust temperature $T = 10$ K, and cosmic-ray ionization rate of hydrogen atoms $\zeta_{\rm CR}^{\rm H} = 1.8 \times 10^{-17}$ s^{-1}. For any total hydrogen column $N_{\rm H}$ and volume density n, we can solve to obtain $f_{\rm mol}$, the molecular fraction. Figure 6 shows, in the n–N plane, the boundary (solid line) between the predominantly atomic and predominantly molecular regimes, which we define by the locus of points for which $f_{\rm mol} = 0.5$.

At any density, we can also define the Jeans length $L_{\rm J} = c_s(\pi/G\rho)^{1/2}$, where $c_s^2 = k_{\rm B}T/\mu$ (we adopt $T = 10$ K). This defines a corresponding total column of gas, $N_{\rm H} = nL_{\rm J}$, that could be expected to be gravitationally bound. The boundary

between gravitationally unbound (low n and N) and bound (high n and N) gas, based on this criterion, is shown in Figure 6 as a dashed line with $n \propto N^2$. Note that if instead of L_J we had chosen as a length scale the diameter D of sphere containing mass equal to the Bonnor–Ebert (Bonnor 1956; Ebert 1957) critical mass, $M_{BE} = 1.182 c_s^3/(G^3\rho)^{1/2}$, then $D = 0.74 L_J$. This would shift the unbound/bound line in the log(N)–log(n) plane to the left by log(0.74) = −0.13.

We note that the gravitational binding criterion discussed above considers only support by thermal pressure. Turbulence can lend further support against gravity, and this is particularly important for molecular gas, which is quite cold. For example, if we considered turbulence-supported clouds with velocity dispersion following the observed linewidth–size relation of Galactic GMCs (Solomon et al. 1987), then the column density separating gravitationally bound from unbound regions would have a constant value equal to half of the mean observed GMC column, amounting to $N_H = 7.5 \times 10^{21}$ cm^{-2}. A higher normalization for the linewidth–size relation (as occurs in galactic center regions; see Oka et al. 2001) would further shift the unbound/bound limit to larger N. Thus, moderate-density molecular gas can, in principle, be gravitationally unbound under conditions of sufficiently high turbulence (Elmegreen 1993). For our current simulations, however, turbulence levels are not this high (see discussion below).

We have denoted three different regions in the log(N)–log(n) plane according to their expected chemical and gravitational properties. The crossing point of the two separation loci is at $n \approx 125$ cm^{-3} and $N_H \approx 1.2 \times 10^{21}$ cm^{-2} ($A_v \sim 0.75$ mag), with the corresponding local Jeans length of $L_J = 3.1$ pc. This size is, in fact, slightly larger than the typical resolution limit of our simulations, $\Delta x = 2$ pc; we show this limit in Figure 6 as a dotted line, with regions to the right resolved and those to the left below the resolution limit. The resolution limit crosses the H I/H_2 separation curve at $n = 180$ cm^{-3}. Because the resolution limit falls at larger N than the bound/unbound separation nearly everywhere in the molecular domain, all zones at a given density that are resolved and molecular would also be gravitationally bound. In practice, clouds do not exceed $\sim$ 100 pc in cross section; we have marked this limit in the figure as a dotted line.

According to the limits shown in Figure 6, any resolved regions in our simulations at $n > 100$ cm^{-3} would be molecular. This is a conservative definition, since it omits some gas between $n \sim 10$ and 100 with $N_H > 10^{21}$ cm^{-2} that could be molecular. However, gas at these densities could also be in the cold atomic phase (which extends down to $n_{cold,min} = 8.6$ cm^{-3} for the cooling curve we adopt); we choose the stricter definition. We note that when the virial ratio ($\sim$ kinetic/gravitational energy; see Paper I) is measured for gas in the range $n = 1$–100 cm^{-3} (most of which is at 10 cm^{-3} < n), the values are well above unity—implying that gas parcels in this density range is mostly found in non-self-gravitating regions with low surrounding column densities, to the left of the unbound/bound curve. This suggests that, in practice, very little high-column density gas that would be molecular is missed when we set the minimum threshold at 100 cm^{-3}. From the point of view of dynamics, this is because the density rises whenever any region becomes gravitationally bound, so low-density regions at high column are rapidly depopulated. We also note that the H_2 formation time in dense, cold regions is expected to be short ($\sim 10^6$ yr from Glover & Mac Low 2007a, 2007b), because supersonic shocks increase the density above ambient values and accelerate the molecule-formation process, which occurs at a rate of nR_f.

4.2. Molecular Mass–Pressure Relation

Following the discussion in the previous section, we adopt a working definition of molecular gas as that at $n_H > 100$cm^{-3}. Atomic gas therefore consists of the lower-density complement, including both what would be observable as warm and as cold H I in 21 cm emission. The mass ratio of molecular to atomic hydrogen is then defined as

$$R_{mol} \equiv \frac{M(n > 100\,\mathrm{cm}^{-3})}{M(n < 100\,\mathrm{cm}^{-3})}, \tag{12}$$

where we apply space and time averages before taking the ratio.

Figure 7 shows R_{mol} as a function of $P_{BR} = \Sigma v\sqrt{2G\rho_*}$ for all hydrodynamic and hydrostatic series (we use $v = 8$ kms^{-1} as in BR06). We also show as a solid line the empirical fitting formula from the observational study of BR06 (see their Equation 13):

$$R_{mol} = \left[\frac{P_{BR}/k_B}{4.3 \times 10^4\,\mathrm{K\,cm}^{-3}}\right]^{0.92}. \tag{13}$$

Interestingly, we find that our results for R_{mol} follow the empirical result for some but not all series. In particular, the models in Series Q and R—which have values of Ω that scale with Σ in such a way as to keep the gaseous Toomre parameter constant—are close to the BR06 fit. The models in Series K, which have constant κ and therefore high (or low) values of κ/Σ where P_{BR} is low (or high, respectively), do not follow the empirical result of BR06, but instead show a ratio R_{mol} that is near unity independent of P_{BR}. This has two interesting implications. First, our models with $\Omega \propto \Sigma$ have similar behavior to real galaxies, indicating that real systems evolve (by converting their gas to stars) in such a way as to have the Toomre parameter fall within a limited range of values. Second, because the K Series departs from the BR06 result, our models suggest that the molecular fraction does not have a one-to-one relationship to the effective pressure parameter P_{BR}. Comparing series Q and K which have the same Σ and ρ_*, R_{mol} increases with increasing κ. For example, Figure 8 shows that R_{mol} increases by a factor of 2.4 when Ω (and κ) increases by a factor of $2\sqrt{2}$, for the highest Σ ($\Sigma = 42\,M_\odot$ pc^{-2}) model. For the $\Sigma = 21\,M_\odot$ pc^{-2} model, the R_{mol} increase is 60% for an Ω increase by a factor of $\sqrt{2}$, comparing the Q and K series. Series S, which varies κ at a given value of Σ and ρ_*, also shows departures from the empirical R_{mol} versus P_{BR} relation.

Given that molecular gas in our models is primarily found in gravitationally bound systems, it in fact makes sense that the molecular fraction should not have a one-to-one relationship to the parameter P_{BR}, since P_{BR} does not include any effects of galactic rotation. Galactic rotation and shear are crucial for regulating the large-scale gravitational instabilities that create GMCs in real galaxies as well as in our models, so we believe that the molecular-to-atomic ratio must intrinsically be sensitive to environmental factors that are not captured in P_{BR}. Thus, if observed galaxies *do* show a one-to-one relation between R_{mol} and P_{BR}, it implies that the environmental parameters κ, Σ, and ρ_* are not all independent in real systems.

In Figure 8, we show R_{mol} as a function of the surface density for all of our model series. The behavior is similar to that shown in Figure 7 because P_{BR} depends monotonically on Σ for all our series: $P_{BR} \propto \Sigma^2$ for Series Q and K (which have $\rho_* \propto \Sigma^2$), while $P_{BR} \propto \Sigma$ for Series R (which has $\rho_* = $ const.).

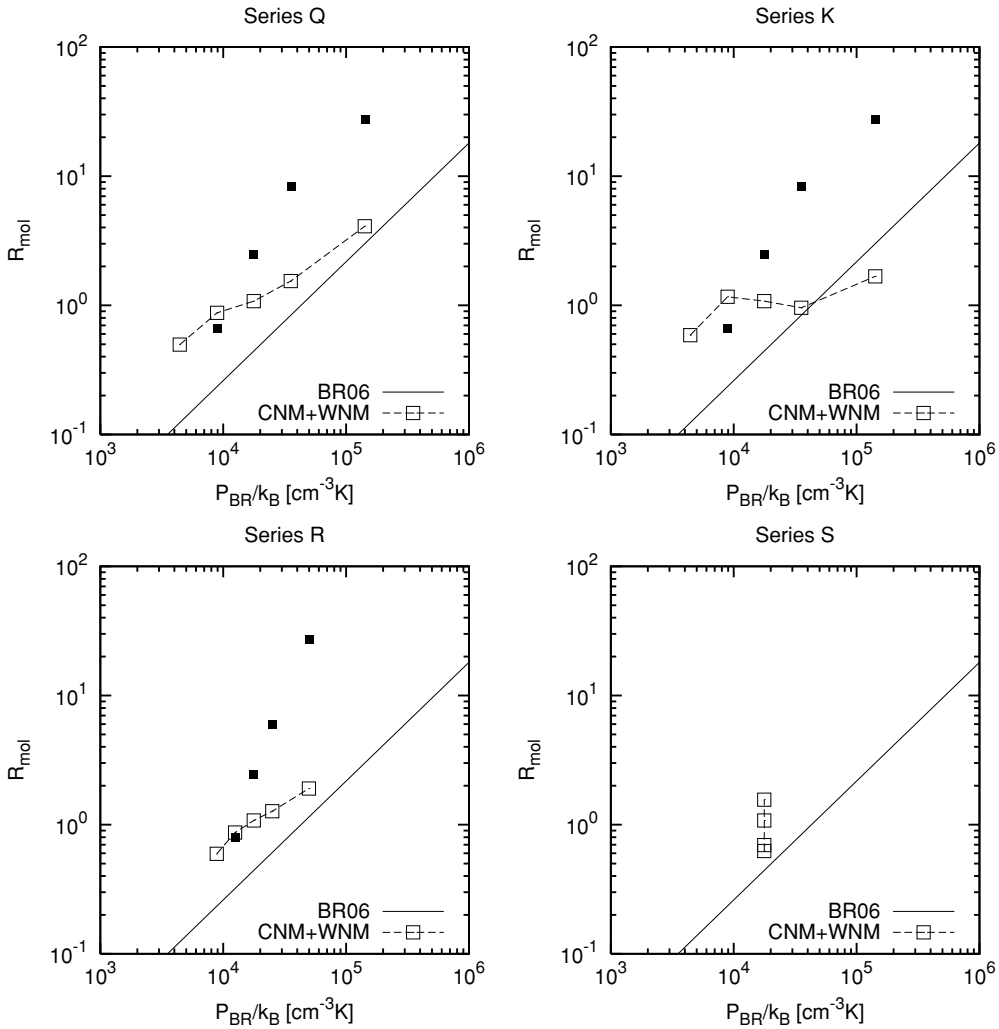

Figure 7. Mean molecular-to-atomic mass ratio $R_{\rm mol}$ as a function of $P_{\rm BR}$ (see Equation 7), shown as open boxes for all hydrodynamic models. Filled boxes show the results from hydrostatic models. The solid line shows the empirical fit from BR06 (Equation 13).

From both Figures Figure 7 and 8, it is evident that the hydrostatic models (filled boxes) generally have a much larger molecular component than both the hydrodynamic models and the empirical results, except at low gaseous surface density. This indicates that turbulence is essential for determining the phase balance between diffuse and dense gas in the ISM as a whole. If the ISM were a static system, it would be overwhelmingly molecular even at fairly moderate values of Σ and ρ_*. In real galaxies, turbulence limits gaseous settling into the midplane and the extreme self-compression that would otherwise ensue.

While we have argued that the molecular content of a galaxy cannot (in general) be predicted solely from Σ and ρ_* because self-gravitating horizontal contraction is also responsive to the local rotation and shear rates, it still is plausible that the molecular fraction should reflect the *true* mean pressure in the ISM. If molecular gas is collected in self-gravitating clouds, then since their internal pressure is higher than ambient levels, an increase in the molecular fraction should go hand-in-hand with a higher mass-weighted mean pressure $\langle P\rangle_\rho$. At the same time, ambient midplane pressures $\langle P\rangle_{\rm midplane}$ increase when the total gas surface density increases, and (provided that κ is low enough) larger Σ also renders the disk susceptible to gravitational instabilities that would form dense, bound clouds and increase the molecular fraction.

We explore these ideas by plotting in Figure 9 the molecular-to-atomic ratio against our two measures of mean gas pressure, $\langle P\rangle_\rho$ and $\langle P\rangle_{\rm midplane}$. We also fit the combined results for all series to single linear relations. These fits, overplotted in Figure 9 as solid and dotted lines, are $R_{\rm mol} = \langle P\rangle_\rho/[7.6\times10^4\ {\rm cm^{-3}K}\,k_{\rm B}]$ and $R_{\rm mol} = \langle P\rangle_{\rm midplane}/[6.7\times10^3\ {\rm cm^{-3}\,K}\,k_{\rm B}]$. For Series Q and R, the fits using $\langle P\rangle_\rho$ are quite good, and the fits using $\langle P\rangle_{\rm midplane}$ are also fairly good (Series Q and R also show better agreement with empirical results than the other series). For Series K, the fit using $\langle P\rangle_\rho$ is reasonably close to the model results, but the fit based on $\langle P\rangle_{\rm midplane}$ fails in a similar manner to that shown in Figure 7 and discussed above. The basic reason for this is that the midplane pressure, either directly measured or estimated using Equation (9), increases with increasing Σ. However, the molecular-to-atomic ratio for Series K does not strongly and secularly increase with Σ due to the differences in rotational effects in this constant-κ series compared to the other series. At high values of Σ in Series K, the disk is extremely gravitationally unstable overall, and as a consequence is more active in producing feedback than other models at the same Σ. As a consequence, a smaller fraction of the gas mass ends up being in the dense phase than in Series Q and R. Overall, we conclude that $R_{\rm mol}$ is indeed well correlated with the mass-weighted mean pressure, $\langle P\rangle_\rho$, as (almost definitionally) is

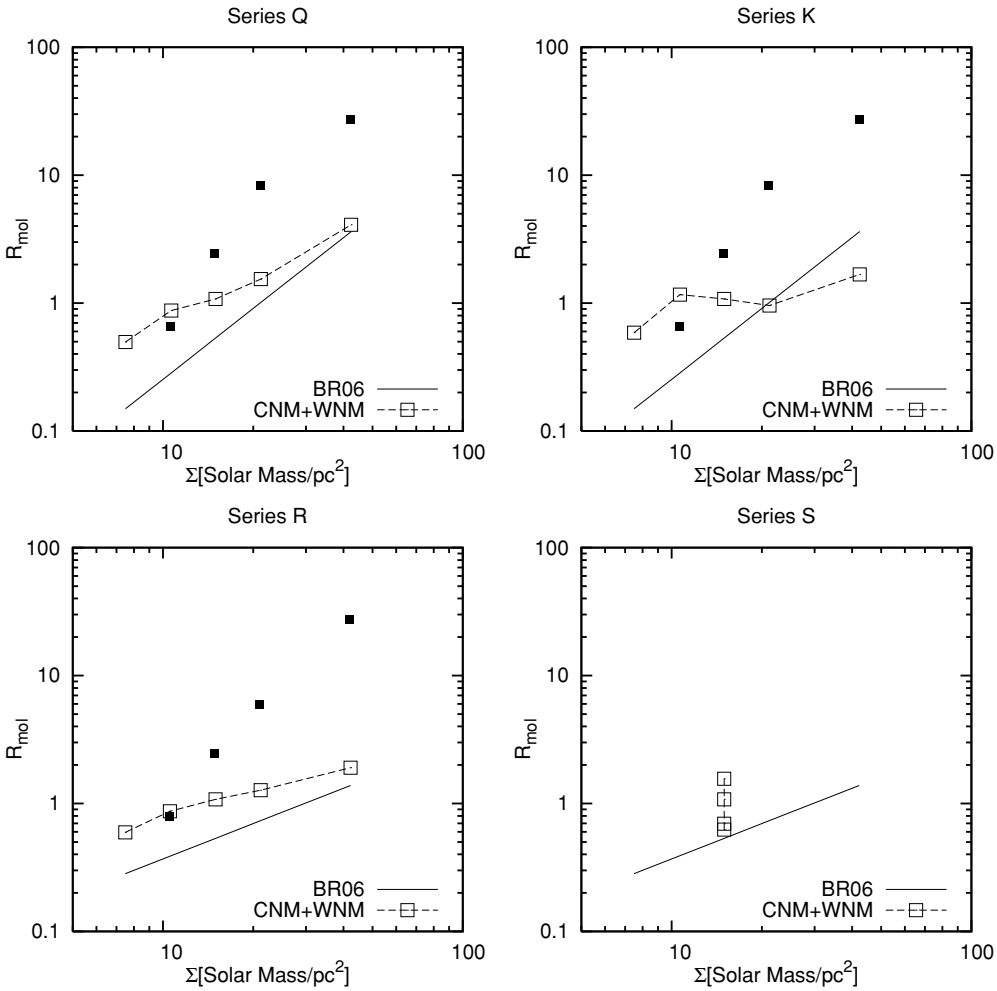

Figure 8. Molecular-to-atomic mass ratio $R_{\rm mol}$ vs. total gaseous surface density Σ. Open boxes show the results from hydrodynamic models, and filled boxes show the hydrostatic model results (HSP for Series K and Q, HSC for Series R). The solid line indicates the empirical result from BR (Equation 13 using Equation 7).

expected. The measured mean midplane pressure, which is more closely related to simple vertical-equilibrium pressure estimates, is less well correlated with $R_{\rm mol}$ when environmental parameters κ, ρ_*, and Σ are all independent.

5. SUMMARY AND DISCUSSION

We have used numerical simulations of turbulent, multiphase, self-gravitating gas orbiting in the disks of model galaxies to study the relationships among pressure, the vertical distribution of gas, and the relative proportions of dense and diffuse gas. In particular, we compare the results on vertical stratification obtained from spacetime averages of fully dynamic—and often turbulence dominated—systems with simple estimates based on single-component effective hydrostatic equilibria. We also investigate how vertical-equilibrium estimates for the pressure compare with measured mean values of the pressure in our models. Empirical studies by BR06 have identified a linear relation between the molecular-to-atomic mass ratio $R_{\rm mol}$ and a midplane ISM pressure estimate, $P_{\rm BR} \propto \Sigma\sqrt{\rho_*}$. We study the origin and implications of this relation by testing the correlations among $R_{\rm mol}$, $P_{\rm BR}$, and the directly measured midplane and mean pressures in our models.

Our chief conclusions, and their implications, are as follows.

1. The average disk scale height is well represented by estimates that assume hydrostatic equilibrium and an effective total pressure based on the total (thermal + turbulent) vertical velocity dispersion (see Figure 3 and Equation 2). Thus, provided that gas surface densities, vertical velocity dispersions, and stellar density can be measured, an accurate estimate for the disk thickness can be obtained.

Hydrostatic equilibrium with an effective turbulent pressure is commonly assumed in both Galactic and extragalactic observational studies (e.g., Lockman & Gehman 1991; Malhotra 1994, 1995; Combes & Becquaert 1997; Olling & Merrifield 2000; Narayan & Jog 2002; Dalcanton et al. 2004; Blitz & Rosolowsky 2004, 2006; Kasparova & Zasov 2008), but to our knowledge the relations that are generally adopted have not previously been tested with direct numerical simulations. Our hydrodynamic studies demonstrate that for determining the scale height H, the effective hydrostatic equilibrium assumption is indeed sufficient, even when turbulent support far exceeds thermal support (and provided that magnetic effects are subdominant; see below). Thus, measured disk thicknesses in edge-on disk galaxies could, in principle, be used to determine the unobservable vertical velocity dispersion, and measured line-of-sight velocity dispersions in face-on galaxies could be used to determine the unobservable disk thickness.

The basic reason the hydrostatic formula can be used to obtain an accurate measure of H is that what is really being equated is the total vertical momentum flux $\rho(k_{\rm B}T/\mu + v_z^2)$ averaged over the midplane, and the total vertical weight of the ISM,

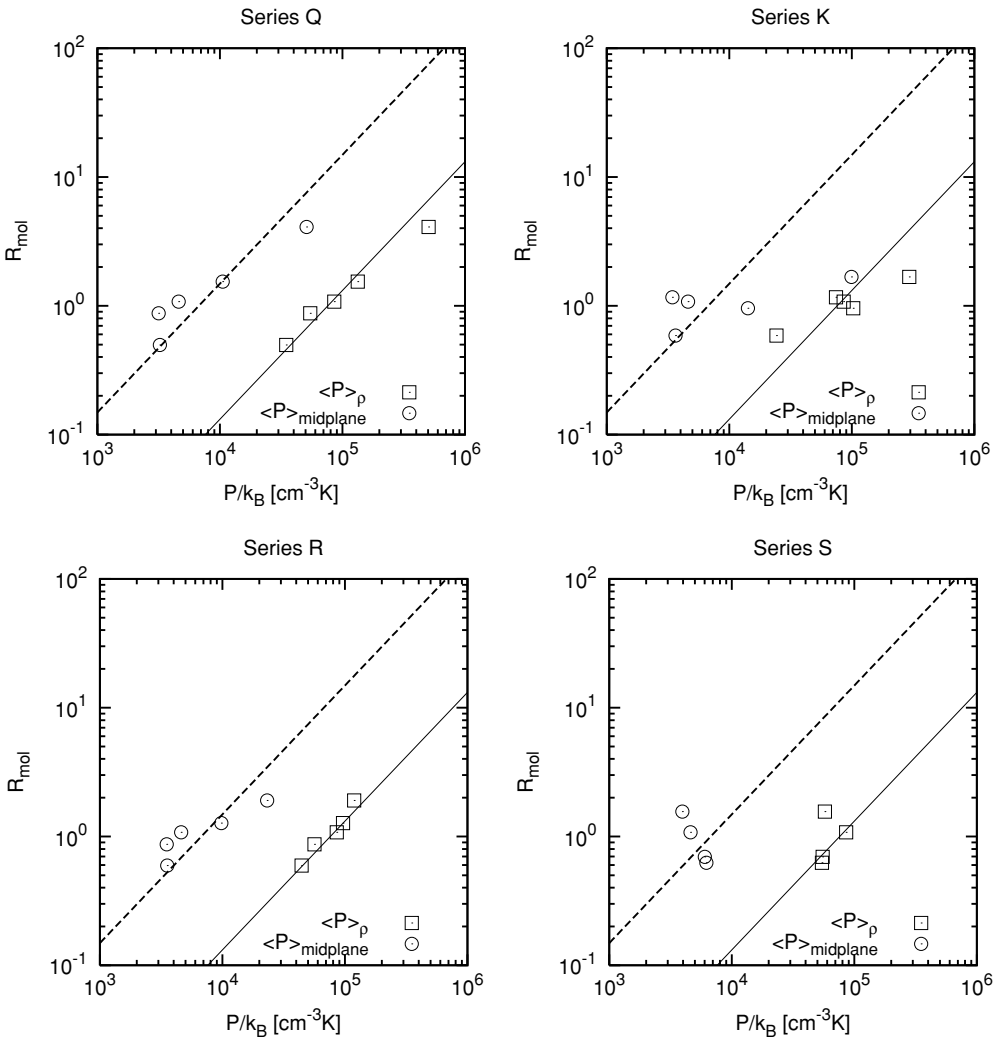

Figure 9. Molecular-to-atomic mass ratio $R_{\rm mol}$ vs. measured mass-weighted mean pressure $\langle P\rangle_\rho$ and midplane pressure $\langle P\rangle_{\rm midplane}$ for all hydrodynamic models. Lines show linear fits (see text).

$\int dz\, \rho\, g_z \sim \rho 4\pi G(\rho+\rho_*)H^2$, averaged over the horizontal direction. Provided that the time-averaged value of the momentum per unit volume in the midplane does not change, momentum conservation including gravitational source terms demands that the difference between vertical momentum flux and vertical weight must be zero, independent of details of the dynamics. The formula $H^2 \approx \sigma_z^2/[4\pi G(\rho_* + \Sigma/H\sqrt{2\pi})]$ is therefore fundamentally an expression of momentum conservation.

2. Mass-weighted mean pressures $\langle P\rangle_\rho$ in our hydrodynamic models significantly differ from the mean midplane pressure $\langle P\rangle_{\rm midplane}$, while these quantities are quite similar to each other in our static comparison models. Typically, the hydrodynamic models yield values of $\langle P\rangle_\rho$ an order of magnitude larger than $\langle P\rangle_{\rm midplane}$. The difference can be attributed to self-gravitating condensation, which makes concentrated clouds with high internal pressure rather than a horizontally uniform gas distribution with more moderate pressure.

Simple estimates of the pressure based on vertical hydrostatic equilibrium fall between mass-weighted and midplane values, with the formula used by BR06 (see our Equation 7) comparable to the geometric mean $P_{\rm BR} \sim \sqrt{\langle P\rangle_\rho \langle P\rangle_{\rm midplane}}$. A single-component estimate for the midplane thermal pressure that accounts for self-gravity and the mean thermal and turbulent velocity dispersions (see Equation 9) follows the measured midplane pressure fairly closely, especially at high Σ. Thus, if turbulent and thermal vertical velocity dispersions can be measured directly (for face-on galaxies), a good estimate of the midplane total or thermal pressure can be computed via Equation (8) or (9). For an edge-on system in which the scale height is measured, the midplane total or thermal pressure can be estimated as $\Sigma/(H\sqrt{2\pi}) \times \langle\sigma_z^2\rangle$ or $\langle c_s^2\rangle$. Midplane pressure estimates based on large-scale observables that assume hydrostatic equilibrium can be quite accurate, but this depends on an accurate measure of the vertical velocity dispersion or vertical thickness. Even if the velocity dispersion is not known, the *relative* midplane pressures of different regions within a galaxy (or from one galaxy to another) can be obtained using the hydrostatic formulae, provided the variation in the (unknown) velocity dispersion within the observational sample is small compared to the variation in the stellar volume and gaseous surface densities. Midplane pressure estimates made in this way should not, however, be treated as a proxy for the pressure in the typical mass element, $\langle P\rangle_\rho$, which can be much larger than the pressure in the typical volume element.

3. Based on calculations of molecular abundance as a function of hydrogen volume density n and column density N combined with the resolution and measured virial ratios in our simulations, we adopt a working definition of gas at $n \geqslant 100\,{\rm cm}^{-3}$ as

"molecular" and $n < 100\,\mathrm{cm}^{-3}$ as "atomic." We then investigate the ratio $R_{\rm mol} = M_{\rm H_2}/M_{\rm H\,I}$ for all our models. We find that Series Q and R, which have rotation rate $\Omega \propto \Sigma$, show correlations between $R_{\rm mol}$ and $P_{\rm BR}$ (or $R_{\rm mol}$ and Σ) that are similar to the empirical result reported by BR06, $R_{\rm mol} \propto P_{\rm BR} \propto \Sigma\sqrt{\rho_*}$. On the other hand, Series K and S, in which Σ and Ω do not vary together, depart from the empirical relation $R_{\rm mol} \propto P_{\rm BR}$.

We conclude that (1) the molecule fraction inherently depends on the rotational state of a galactic disk, not just on the local values of the stellar volume and gaseous surface densities ρ_* and Σ; and (2) the empirical relation $R_{\rm mol} \propto P_{\rm BR}$ identified by BR06 implies that the third "environmental parameter," the epicyclic frequency $\kappa = \sqrt{2}\Omega$ (assuming a flat rotation curve), is not independent of ρ_* and Σ in real galaxies. This dependence can be accomplished by evolution: for example, disk galaxies may convert gas into stars until they reach a state in which the Toomre parameter $\propto \kappa/\Sigma$ approaches a critical value.

4. We have tested the correlation between $R_{\rm mol}$ and the measured pressures in our models, $\langle P\rangle_{\rm midplane}$ and $\langle P\rangle_\rho$, and find a good correlation in all series only for the latter. The correlation between $\langle P\rangle_\rho$ and $R_{\rm mol}$ is potentially useful as a way to estimate the typical internal pressure within gravitationally bound regions when only the total molecular-to-atomic mass is easily accessible, as for low-resolution observations. This internal pressure is important in the small-scale aspects of star formation such as determining the IMF (McKee & Ostriker 2007), as well as in molecular chemistry. The lack of correlation between $R_{\rm mol}$ and $\langle P\rangle_{\rm midplane}$ in Series K implies that the molecular content cannot, in general, be predicted solely from Σ and ρ_* (i.e., without knowledge of κ), as noted above. This reflects the fact that the formation of self-gravitating clouds is regulated not just by gravitational processes and pressure, but also by angular momentum.

5. For our nonturbulent comparison models, we find that $R_{\rm mol}$ far exceeds observed values. This indicates that turbulence is essential to setting the observed phase balance in the ISM. Recent theoretical investigations of the origin of Kennicutt–Schmidt laws have focused on the dependence of star formation rates on the molecular, rather than total, gas surface density (e.g., Narayanan et al. 2008; Robertson & Kravtsov 2008). Since turbulence is crucial in determining the abundance of dense gas, in simulations that aim to compute this abundance realistically it is necessary to incorporate the feedback effects that drive turbulence, and to run on a fine enough mesh (or with sufficient smoothed particle hydrodynamics particles) that the turbulence is well resolved. While technically challenging in global disk models, local models may offer a more immediate route to this goal.

Caveats. The models analyzed in this paper are subject to a number of limitations, which could potentially affect some of our conclusions. The chief limitations of the simulations are that (1) they are two dimensional, representing cuts in the R–z plane, rather than three dimensional; (2) we have adopted a very simple model to implement turbulent driving as a star formation feedback effect from H II regions, and we have not included other drivers of turbulence such as supernovae, spiral shocks, and shear instabilities; and (3) we have not included magnetic fields (or cosmic rays). We intend to pursue these extensions in future work.

Inclusion of magnetic fields and altered turbulent driving would certainly affect the specific quantitative findings for $H_{\rm ave}$, $\langle P\rangle_{\rm midplane}$, $\langle P\rangle_\rho$, and $R_{\rm mol}$ in our models. We believe, however, that the results we have emphasized regarding physical *relationships* are robust. In particular, with appropriate modifications to include magnetic stresses, the time-averaged vertical momentum flux through the midplane must still equal the time-averaged vertical weight if the mean vertical momentum is conserved. This can be used to predict the total midplane pressure (including the magnetic pressure) and H given the values of Σ, ρ_*, and the thermal, turbulent, and Alfvén velocities. Thus, we anticipate that inclusion of magnetic fields and alternate turbulence sources would not fundamentally alter the conclusion that reasonable estimates of scale heights can be made using observable quantities even in highly dynamic systems.

Further, we expect that our conclusions regarding the presence or absence of correlations between $R_{\rm mol}$ and $\langle P\rangle_\rho$ or $\langle P\rangle_{\rm midplane}$ would continue to hold in models that include additional turbulence sources and magnetic fields, although the details of correlations might change. Namely, angular momentum inherently must be important in permitting or preventing formation of dense, self-gravitating clouds. Our present models account for angular momentum effects, and show that $R_{\rm mol}$ does not in general have a one-to-one relationship with $\langle P\rangle_{\rm midplane}$ or $\Sigma\sqrt{\rho_*}$; we expect this result would carry over into any model that incorporates sheared background rotation of the galactic disk. Thus, if a one-to-one relationship between $R_{\rm mol}$ and $\Sigma\sqrt{\rho_*}$ indeed exists empirically, it implies that Σ, ρ_*, and κ are not all independent quantities in real galaxies.

The authors are grateful to the referee for a number of comments that have helped improve our presentation. Numerical computations used in this project were carried out on the OIT High Performance Computing Cluster, and the CTC cluster in the Department of Astronomy, at the University of Maryland. This work was supported by grant NNG05GG43G from NASA; author H.K. was also supported in part by NSF grant AST 0540450 to the LMA at UMD.

APPENDIX

VERTICAL EQUILIBRIUM WITH STELLAR AND GAS GRAVITY

The vertical momentum equation, when averaged over a horizontal plane, is given by

$$\frac{\partial}{\partial t}\langle \rho v_z\rangle + \frac{\partial}{\partial z}\left\langle P + \rho v_z^2 + \frac{\mathbf{B}\cdot\mathbf{B}}{8\pi} - \frac{B_z^2}{4\pi}\right\rangle = -\left\langle \rho\frac{\partial \Phi}{\partial z}\right\rangle \quad \text{(A1)}$$

(see e.g., Piontek & Ostriker 2007). Here, $\mathbf{B}$ is the magnetic field and Φ is the total (stellar plus gaseous) gravitational potential. In steady state $\langle \rho v_z\rangle$ is time independent, so if we neglect magnetic fields and assume that ρ, v_z^2, $c_s^2 = P/\rho$, and $\partial\Phi/\partial z$ are statistically independent quantities, we obtain

$$\frac{1}{\langle\rho\rangle}\frac{\partial}{\partial z}\left[\left\langle c_s^2 + v_z^2\right\rangle\langle\rho\rangle\right] = -\frac{\partial\langle\Phi\rangle}{\partial z}. \quad \text{(A2)}$$

The Poisson equation, also averaged over the horizontal plane and assuming $R\Omega$ is independent of R, is

$$\frac{\partial^2\langle\Phi\rangle}{\partial z^2} = 4\pi G(\langle\rho\rangle + \rho_*), \quad \text{(A3)}$$

where ρ_* is the background stellar density.

If we now define $\sigma_z^2 = \langle c_s^2 + v_z^2 \rangle$ and assume that this total velocity dispersion is independent of height z, we can combine the vertical momentum equation with the Poisson equation to obtain a second-order differential equation for the density profile $\langle \rho \rangle \rightarrow \rho(z)$:

$$\frac{\partial}{\partial z}\left(\frac{\sigma_z^2}{\rho(z)}\frac{\partial \rho(z)}{\partial z}\right) = -4\pi G\left(\rho_* + \rho(z)\right). \quad \text{(A4)}$$

Henceforth, we assume that ρ_* is uniform within the gas disk, which is a good approximation provided that the stellar scale height is significantly larger than the gaseous scale height. Equation (A4) is the expression for effective hydrostatic equilibrium in the vertical direction.

Introducing a variable $f(z) = \ln(\rho(z)/\rho_*)$ and a constant $h^2 = \sigma_z^2/(4\pi G\rho_*)$, we have

$$f'' = -\frac{1}{h^2}(1 + e^f), \quad \text{(A5)}$$

where the prime denotes a z derivative. This can be integrated once as

$$\frac{(f')^2}{2} = -\frac{1}{h^2}(f + e^f) + \text{const.} = \frac{1}{h^2}\left(f_0 - f + e^{f_0} - e^f\right), \quad \text{(A6)}$$

where $f_0 = \ln(\rho_0/\rho_*)$ is the boundary condition at the midplane where $f' = 0$. If we Taylor expand and retain only the two lowest order terms, i.e., $f(z) = f_0 - f_1 z^2$ so that $\rho/\rho_0 = \exp(-f_1 z^2)$, the governing ODE becomes an algebraic equation:

$$\frac{(2f_1 z)^2}{2} = \frac{z^2}{h^2}\left(f_1 + \frac{\rho_0}{\rho_*}f_1\right) = \frac{4\pi G(\rho_0 + \rho_*)}{\sigma_z^2} f_1 z^2. \quad \text{(A7)}$$

The coefficient f_1 is

$$f_1 = \frac{1}{2H^2}, \quad H^2 = \frac{\sigma_z^2}{4\pi G(\rho_* + \rho_0)}. \quad \text{(A8)}$$

Therefore, the gas density and pressure are approximately given by Gaussian profiles

$$\rho(z) = \rho_0 e^{-\frac{z^2}{2H^2}}, \quad P(z) = P_0 e^{-\frac{z^2}{2H^2}}, \quad \text{(A9)}$$

where $P_0 = \sigma_z^2 \rho_0$. The midplane gas density ρ_0 is determined by requiring that the profile integrates to the (known) gas surface density,

$$\Sigma = \int_{-\infty}^{\infty} \rho(z)\, dz = \sqrt{2\pi}\rho_0 H. \quad \text{(A10)}$$

Substituting for ρ_0 in Equation (A8), the scale height H must satisfy

$$H^2 = \frac{\sigma_z^2}{4\pi G(\rho_* + \frac{\Sigma}{\sqrt{2\pi}H})}. \quad \text{(A11)}$$

This yields a quadratic equation for H, with solution given by Equation (2) of the text.

REFERENCES

Blitz, L., & Rosolowsky, E. 2004, ApJ, 612, L29
Blitz, L., & Rosolowsky, E. 2006, ApJ, 650, 933
Bonnor, W. B. 1956, MNRAS, 116, 351
Combes, F., & Becquaert, J.-F. 1997, A&A, 326, 554
Dalcanton, J. J., Yoachim, P., & Bernstein, R. A. 2004, ApJ, 608, 189
Dobbs, C. L. 2008, MNRAS, 391, 844
Dobbs, C. L., Glover, S. C. O., Clark, P. C., & Klessen, R. S. 2008, MNRAS, 389, 1097
Ebert, R. 1957, Z. Astrophys., 42, 263
Elmegreen, B. G. 1993, ApJ, 411, 170
Glover, S. C. O., & Mac Low, M.-M. 2007a, ApJS, 169, 239
Glover, S. C. O., & Mac Low, M.-M. 2007b, ApJ, 659, 1317
Heitsch, F., Burkert, A., Hartmann, L. W., Slyz, A. D., & Devriendt, J. E. G. 2005, ApJ, 633, L113
Heitsch, F., Slyz, A. D., Devriendt, J. E. G., Hartmann, L. W., & Burkert, A. 2006, ApJ, 648, 1052
Hennebelle, P., & Audit, E. 2007, A&A, 465, 431
Hennebelle, P., Audit, E., & Miville-Deschênes, M.-A. 2007, A&A, 465, 445
Hennebelle, P., Banerjee, R., Vázquez-Semadeni, E., Klessen, R. S., & Audit, E. 2008, A&A, 486, L43
Hollenbach, D., & McKee, C. F. 1989, ApJ, 342, 306
Kasparova, A. V., & Zasov, A. V. 2008, Astron. Lett., 34, 152
Kim, C.-G., Kim, W.-T., & Ostriker, E. C. 2008, ApJ, 681, 1148
Kim, W.-T., & Ostriker, E. C. 2001, ApJ, 559, 70
Kim, W.-T., & Ostriker, E. C. 2002, ApJ, 570, 132
Kim, W.-T., & Ostriker, E. C. 2006, ApJ, 646, 213
Kim, W.-T., & Ostriker, E. C. 2007, ApJ, 660, 1232
Kim, W.-T., Ostriker, E. C., & Stone, J. M. 2002, ApJ, 581, 1080
Kim, W.-T., Ostriker, E. C., & Stone, J. M. 2003, ApJ, 599, 1157
Klessen, R. S., Heitsch, F., & Mac Low, M.-M. 2000, ApJ, 535, 887
Koyama, H., & Inutsuka, S. 2002, ApJ, 564, L97
Koyama, H., & Ostriker, E. C. 2009, ApJ, 693, 1316
Li, Y., Mac Low, M.-M., & Klessen, R. S. 2005, ApJ, 620, L19
Li, Y., Mac Low, M.-M., & Klessen, R. S. 2006, ApJ, 639, 879
Lockman, F. J., & Gehman, C. S. 1991, ApJ, 382, 182
Mac Low, M.-M. 1999, ApJ, 524, 169
Malhotra, S. 1994, ApJ, 433, 687
Malhotra, S. 1995, ApJ, 448, 138
McKee, C. F., & Ostriker, E. C. 2007, ARA&A, 45, 565
Narayan, C. A., & Jog, C. J. 2002, A&A, 394, 89
Narayanan, D., Cox, T. J., Shirley, Y., Dave, R., Hernquist, L., & Walker, C. K. 2008, ApJ, 684, 996
Oka, T., Hasegawa, T., Sato, F., Tsuboi, M., Miyazaki, A., & Sugimoto, M. 2001, ApJ, 562, 348
Olling, R. P., & Merrifield, M. R. 2000, MNRAS, 311, 361
Piontek, R. A., & Ostriker, E. C. 2007, ApJ, 663, 183
Robertson, B. E., & Kravtsov, A. V. 2008, ApJ, 680, 1083
Solomon, P. M., Rivolo, A. R., Barrett, J., & Yahil, A. 1987, ApJ, 319, 730
Stone, J. M., Ostriker, E. C., & Gammie, C. F. 1998, ApJ, 508, L99
Tielens, A. G. G. M., & Hollenbach, D. 1985, ApJ, 291, 722
Vázquez-Semadeni, E., Gómez, G. C., Jappsen, A. K., Ballesteros-Paredes, J., González, R. F., & Klessen, R. S. 2007, ApJ, 657, 870
Wong, T., & Blitz, L. 2002, ApJ, 569, 157